Sensor and Simulation Notes
Note 460

1 October 2001

DESIGN AND SETUP OF A SHORT PULSE SIMULATOR FOR SUSCEPTIBILITY INVESTIGATIONS

F. Sabath, D. Nitsch
Wehrwissenschaftliches Institut für Schutztechnologien – ABC-Schutz,
Munster (Germany)

M. Jung, Th. H. G. G. Weise
Rheinmetall W&M GmbH,
Unterlüß (Germany)

ABSTRACT **In this paper the setup of a short pulse simulator system for susceptibility investigations is presented. The system consists of a compact ultra wide band UWB source and a half Impulse Radiating Antenna (half IRA). First measurements of the system are compared with calculated field values. The application of interest is the generation of a ultra short pulse with a high electromagnetic field strength.**

Index Terms: Reflector antenna, short pulse, UWB-simulator

I. INTRODUCTION

Modern electronic equipment is of vital importance for the function of airplanes, safety systems and communication. A malfunction in one of these areas could cause severe problems and economic disaster. Therefore the susceptibility of modern electronic systems to fast transient electromagnetic fields like EMP and UWB pulses is of great interest.

For the investigation of the effects of short pulses on modern electronic systems the generation of a fast transient field with high magnitude is a necessary part. For susceptibility investigations of intermediate systems we have built a simulator consisting of a reflector type IRA driven by a high voltage pulser with a risetime of less than 500 ps and an output voltage higher than 100 kV.

To achieve the required pulse shape we have used a dielectric lens to transform the plane wave inside the coaxial system into a spherical wave launched at the feed. Based on the calculated field distribution and an estimation of the transfer losses of the lens the radiated field was computed and compared with measured data.

II. UWB SOURCE

A. High voltage generators

In order to generate high voltage pulses with voltage amplitudes of several 100 kV's two major technologies are known: Marx Generators, and Tesla Transformers. We began our investigations with a 6 stage Marx Generator with an output voltage of 150 kV and changed to the Tesla Transformer technology for the following reasons: compact size, low input voltage on the primary side, low energy requirements of the pulser,

capability to operate easier on higher repetition rates. The difference between these two high voltage generator concepts are shown in figure 1. Especially the low pulse energy requirements for the generation of UWB pulses with risetimes < 500 ps and pulse widths < 1 ns give the Tesla Transformer an advantage against the Marx Generator. Our source system generates an output voltage well above 100 kV out of an input voltage of less than 5 kV. Figure 2 shows the voltage waveform of the primary and the secondary side of the older Tesla Transformer.

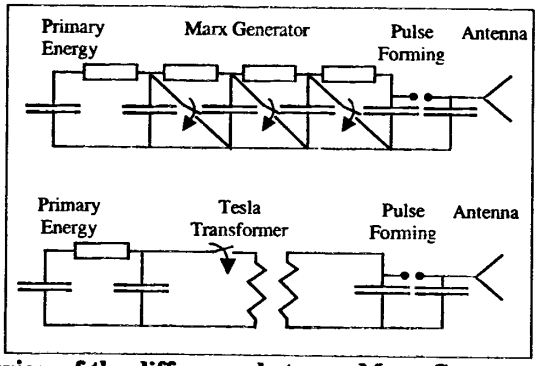

Figue-1: Overview of the difference between Marx Generator and Tesla Transformer UWB sources

Typical for the Tesla Transformer principle is, that the primary energy is transferred step by step to the secondary side, due to the low coupling factor between the inductivities of the primary and secondary side. It can be observed via the increase of the voltage amplitude at the secondary side. To achive optimal performance of the Tesla Transformer the gap between the frequency of the primary side and the secondary side should as small as possible. Therefore all stray capacitances and inductivities must be taken into account during the system design.

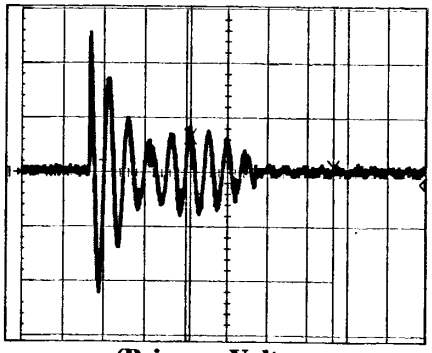

(Primary Voltage 2 kV/div, 2 µs/div)

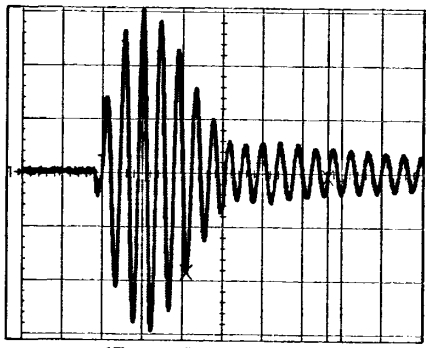

(Secondary Voltage 20 kV/div, 2 µs/div)

Figure-2: Voltage waveform on primary (left) and secondary side (right) of the Tesla Transformer

B. Pulse forming system

The generation of pulse rise times less < 500 ps at pulse amplitudes above 100 kV via gas or oil discharge is generally done by fast overcharging of a spark gap. Because of the fact, that a fast overcharging leads to a much higher voltage of the gap than a slow charging, there is a higher electrical field strength inside the gaps. By using several gaps in series, the leading edge of the pulse could be sharpened [2].

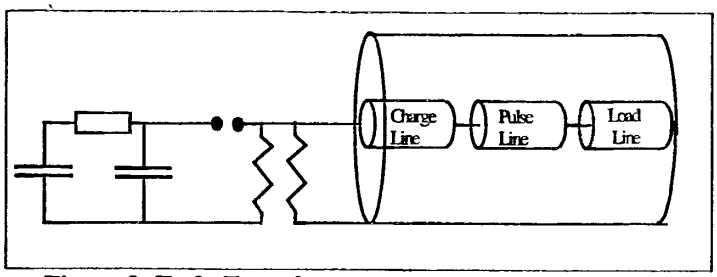

Figure 3: Tesla Transformer and pulse forming system

We designed a pulse forming system consisting of three sections, a charging line, a pulse line, and a load line for basic investigations (see Figure 3). Each line is separated from the other by a discharge gap. At the last gap the electrical field strength between the electrodes can reach more than 1 MV/cm before the spark is ignited. Each line is designed as a 50 Ω pulse line of a certain length. In each line a capacitive voltage probe is placed to measure the voltage. The system is designed to operate at pressures up to 20 bar. Figure 4 show a pulse shape of the voltage in the middle of the pulse line. In this example the rise time is about 500 ps. By changing the electrode gap and the pressure a minimum voltage risetime of less than 300 ps can be achived at an input voltage of more than 100 kV.

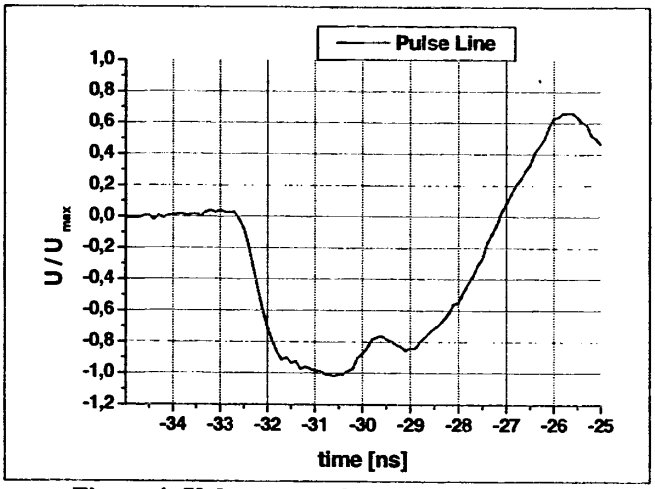

Figure 4: Voltage waveform at the pulse line

III. ANTENNA

Short pulse systems are in need of special impulse radiating antennas, because ordinary wideband antennas are not able to radiate short high magnitude pulses due to their dispersion. There are several antenna designs (e. g. reflector IRA or TEM horn antenna) available for impulse radiating applications [4].

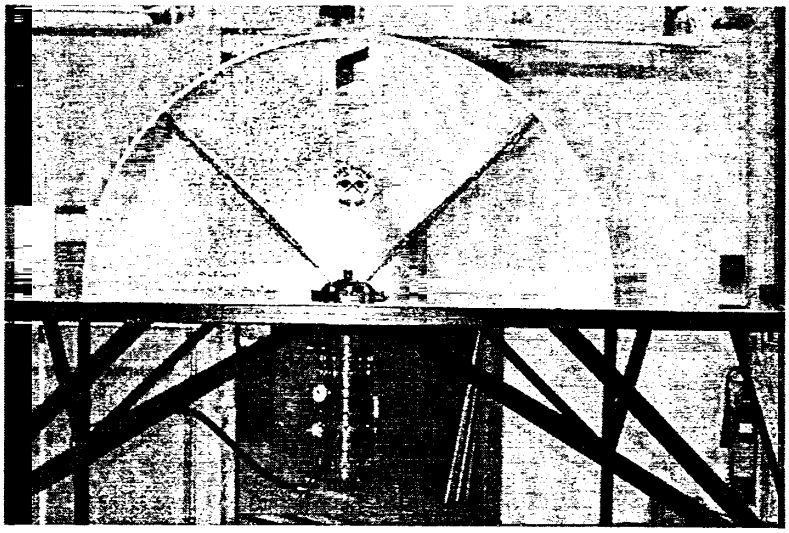

Figure 5: Half IRA with the compact gas switch UWB pulser

A. Construction Details

For our simulator we used a reflector type IRA design consisting of a parabolic reflector with a diameter of D = 1.8 m and a focus length of F = 0.755 m. In order to minimize the disturbance of the radiated field by the large pulser system, the antenna was built as a half IRA (Figure 5). The half IRA design operates with one half of the antenna and we used a metal plate, at the symmetry plane, as a mirror for the electromagnetic field and for the electromagnetic decoupling of the space below and above the metal plate. The antenna is fed by a TEM feed consisting of two triangular metallic plates, whose impedance is given by [5]:

$$Z_{Feed} = \sqrt{\mu/\varepsilon} \cdot \frac{K(m)}{4 \cdot K(1-m)} \tag{1}$$

with

$$m = \frac{\tan^2\left(\beta_i/2\right)}{\tan^2\left(\beta_a/2\right)}$$

where K(m) is the complete elliptic integral of the first kind. The disturbance of the field distribution can be minimized if the edge to the reflector dish connects the symmetry point of the current distribution on the feed arms. To specify the relevant design parameters the angles β_i and β_a for various feed impedances are depicted in Figure 7. In case the feed impedance matches the 50 Ω impedance of the source, the values for the angles are $\beta_a = 109°$ and $\beta_i = 32°$. For the realization of the feed arms the extremely large value for β_a leads to several problems. To minimize the aperture blockage by the feed arms and to get an uncomplicated termination network we limited the outer angle to $\beta_a = 80°$.

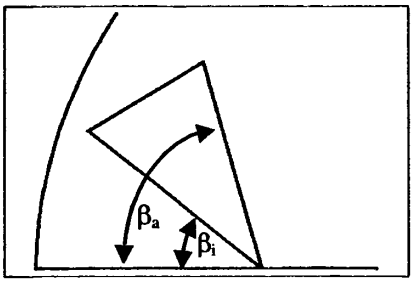

Figure 6: Angles for specifying the feed arm angles

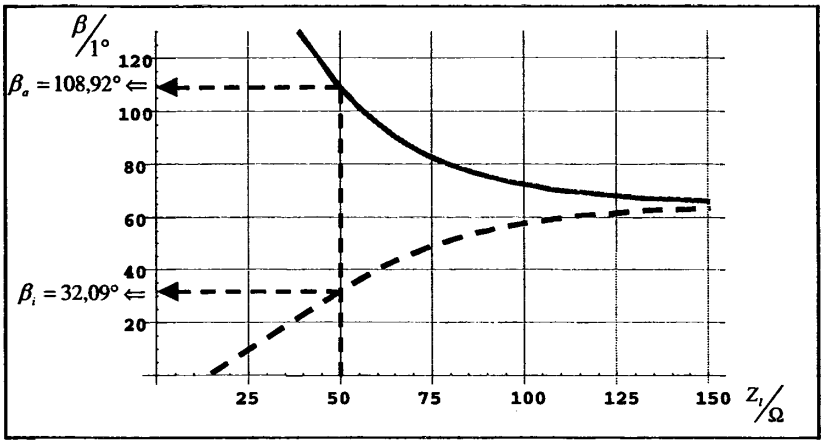

Figure 7: Design angles of the feed arms as a function of the feed impedance (solid line: β_a; dashed line: β_i)

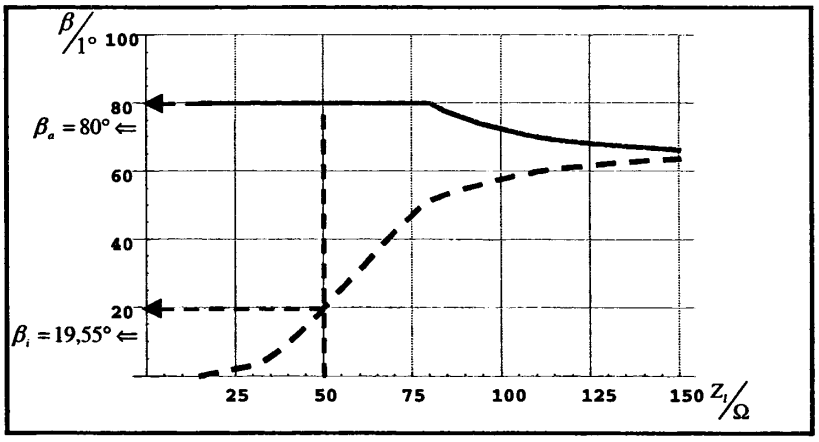

Figure 8: Modified design angles (solid line: β_a; dashed line: β_i)

The modified values for the relevant angles are shown in Figure 8. In this diagram it can be seen clearly that for impedances below 80 Ω the upper angle is identical to the given limit. For the case of Z_L=50 Ω we obtain the remaining inner angle β_i = 20°. Some comments about the modification of the design angle. As a result of limiting β_a the current symmetry angle decreased and did not match the edge of the reflector dish. For higher voltage levels of the source the electric strength inside the feed was an important

design aspect. By decreasing the angle β_i the distance between the lower edge of the feed arms and the metallic plane and the electric stand off also decreases. As a result it was necessary to modify the region near the apex.

The most complicated part of the antenna design is the adaptation between the coaxial source system and the feed of the antenna. In general, one intends to keep this electrically small, but the high voltage denies this possibility. In order to solve the problem we inserted a feed point lens at the connection between the source and the beginning of the feed arms (Figure 9). The effect of the lens is to convert the plane wave inside the coaxial source system to a spherical wave launched onto the feed arms. The focus of the spherical wave is on the ground plane, matching the focus of the parabolic reflector.

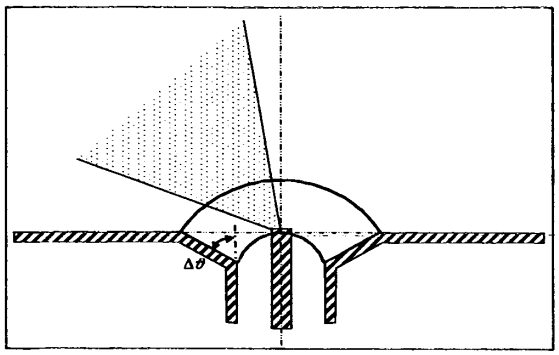

Figure 9: Principe of the feed point lens

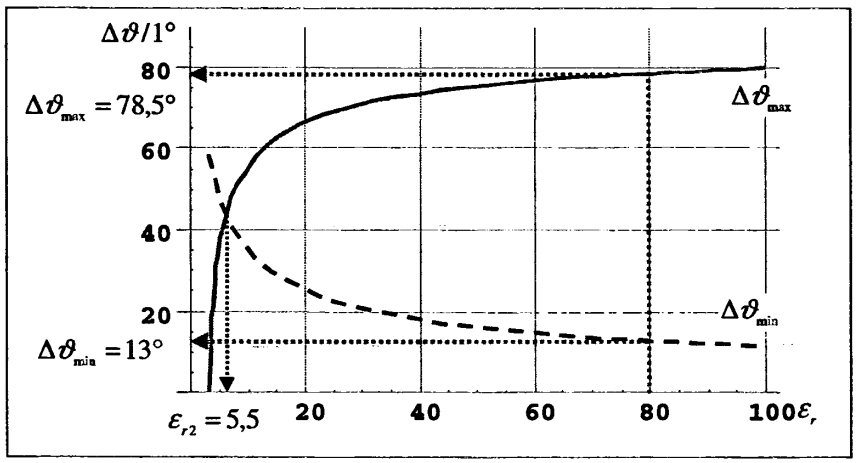

Figure 10: Opening angle of the lens as a function of the permittivity. (solid line: $\Delta\theta_{max}$; dashed line: $\Delta\theta_{min}$)

The transmission of the electric field at the surface from the plastic used in the source system ($\varepsilon_r = 3.18$) and the lens material as well as the transmission from the lens to the air inside the feed limit the opening angle $\Delta\theta$. To choose the dielectric material of the lens, the upper and lower limits of $\Delta\theta$ were calculated and depicted in Figure 10 as a function of the permittivity ε_{rl} of the lens material. It can be seen that there is a crossover at $\varepsilon_{rl} = 5.5$, below which no solution is possible. Other restrictions of the material are the high electric stand off and the ultra wide band spectrum of the voltage signal and the mechanical behavior. Most materials with a constant permittivity of $\varepsilon_{rl} < 5.5$ do not have the necessary electric stand off. With respect to a low budget realization we made the lens out of deionized water, covered by a plastic cap. Due to the high permittivity of water ($\varepsilon_r = 80$) reflections will occur at both surfaces of the lens. By calculating the reflections at the dielectric step from plastic ($\varepsilon_r = 3.18$) to water ($\varepsilon_r = 80$) we are able to estimate the capabilities of an optimal design, that uses a lens permittivity near 5.5.

B. Estimation of the radiation behavior

Assuming a pure TEM wave, the electrical field strength launched at the feed can be calculated via conformal mapping and by using the complex electric potential. Based on the known behavior of a parabolic reflector we compute the electric field inside the aperture. The effects of the lens were modeled by a dielectric wall of 5 cm thickness. Based on the aperture field and assuming far field conditions we computed the radiated field for an ideal full IRA (Figure 11; solid line) and a half IRA with finite size plane (dashed line). A detailed description of the calculation may be found in [7] and is not repeated here.

The normalized magnitude of the radiated field in the vertical plane is shown in Figure 11 as a function of the direction angle. Due to the reflection on the finite size plane the field radiated from the real half IRA is increasing for small direction angles. This behavior leads to a beam direction which differs from boresight.

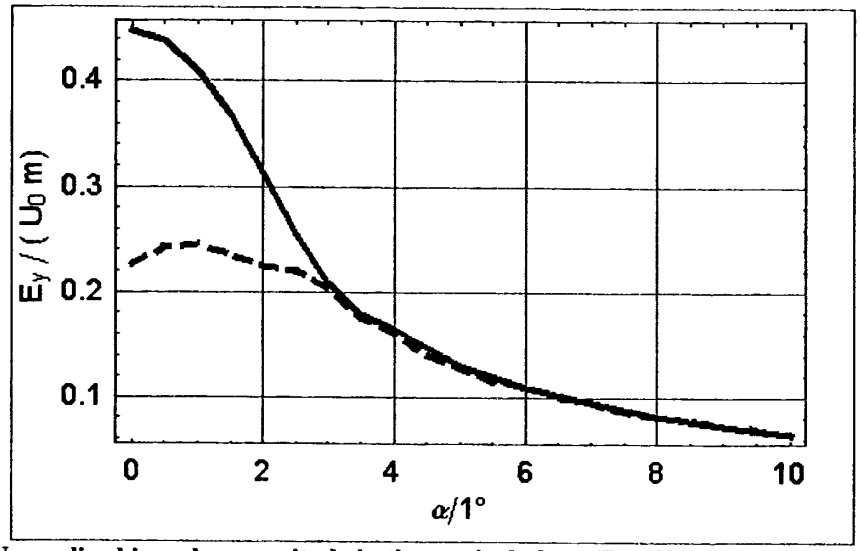

Figure 11: Normalized impulse magnitude in the vertical plane (R = 40 m, solid line: ideal full IRA, dashed line: half IRA)

VI. RESULTS

As the first step of the comparison between the predicted behavior and measured data we measured the reflected voltage level using a TDR setup. Figure 12 shows the measured reflection ratio of two configurations: with and without water inside the lens. The measurements without water (thin line) are demonstrating the good fit between the characteristic impedance of the source ($t < 0$) and the feed arms ($1\ ns < t < 6\ ns$). Compared to this the measurements including the water differs significantly. The deviations between both curves can be explained using our simple lens model (dielectric wall). The reasonable agreement between the predicted reflection levels on a dielectric wall (dashed line) and the water filled lens setup clarifies, that the reflections observed are only reflections at both surfaces of the lens. As a result of these reflections the transfer ratio of the lens can be determined to 0.6. The TDR measurements clarify also that the delay time between two reflections is $\Delta\tau = 3$ ns.

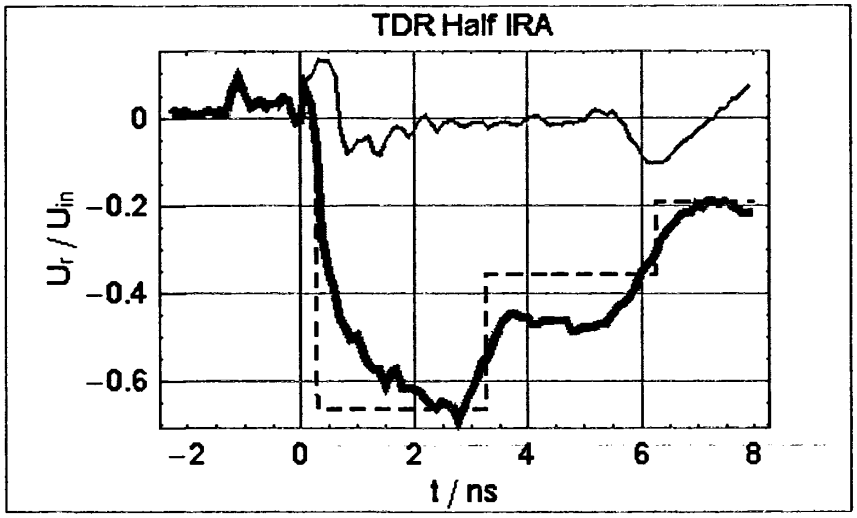

Figure 12: Reflected voltage levels of the half IRA (thin: without water, thick: with water; dashed: predicted values)

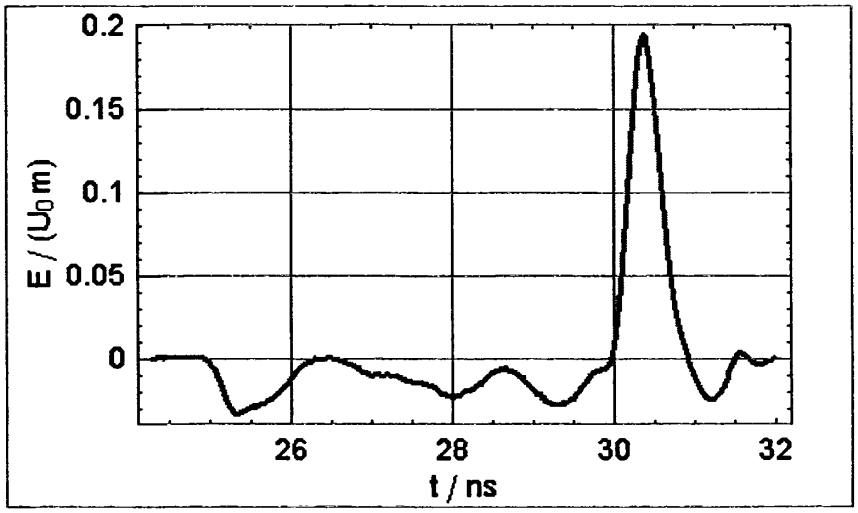

Figure 13: Field response on a double exponential test impulse (τ_r = 0.1 ns, T_{FWHM} = 2.5 ns)

The radiated field of the system was measured at a distance of R = 11 m in both the vertical and the horizontal plane. Figure 13 shows the response of the UWB-antenna on a double exponential test pulse with a rise time of τ_r = 0.1 ns. The prepulse with the shape of the test signal can be observed at t = 25 ns. 5 ns later, a time which correspond with the focus length F = 0.755 m, the main pulse can be seen clearly. At t = 28 ns we observed also the prepulse of the field signal of the first reflection inside the lens.

Due to the rise time of the test signal we expect a pulse duration of T_{FWHM} = 0.1 ns. The measured pulse duration of T_{FWHM} = 0.65 ns indicates that the measurements were performed under near field conditions. Based on the short rise time and the diameter of the reflector we calculate the beginning of far field at a distance of R_{far} = 40 m.

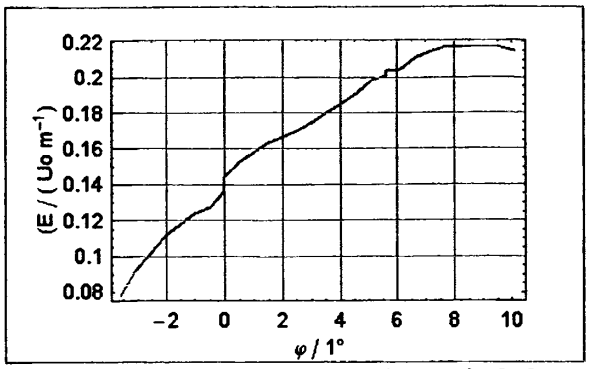

Figure 14: Peak electric field in the vertical plane

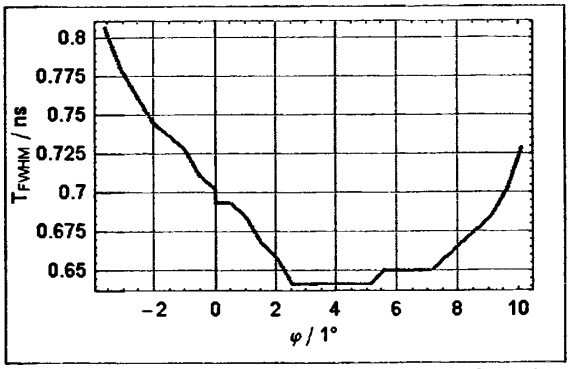

Figure 15: Pulse duration (T_{FWHM}) as a function of the direction angle in the vertical plane

The peak electric field values $\hat{E}$ measured in the vertical plane are plotted in Figure 14 as a function of the direction angle. Measurement points below the level of the metallic plate are indicated by negative direction angles $\varphi_v < 0°$. Due to the blockage effect of the metallic plate a step of the curve can be observed at $\varphi_v = 0°$. Based on the far field calculation we expect the main beam and the maximum peak values at $\varphi_v = 1.5°$, but we observed the maximum values at the direction $\varphi_v = 8°$. In a rough interpretation one could identify these angles as the direction of the main beam. The failure of such simple interpretation can be demonstrated considering the pulse duration (Figure 15). The minimum pulse duration of $T_{FWHM} = 0.65$ is 6 times larger than the rise time of the test pulse. This makes clear that the measurement conditions are way off from the far field. The shortest radiated field pulse occurs at the direction $\varphi_v = 4°$. Under far field condition both the shortest pulse duration and the maximum peak value identify the main beam. But due to near field effects (impact of the metallic plane, etc.) we found that the pulse duration will be a better measure for the main beam direction than the maximum peak electric field. A possible reason for the difference between the predicted and the measured direction of the main beam could be the uncertainties of the production process.

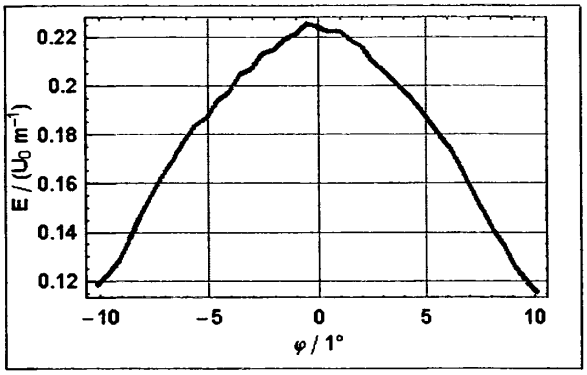

Figure 16: Peak electric field in the horizontal plane

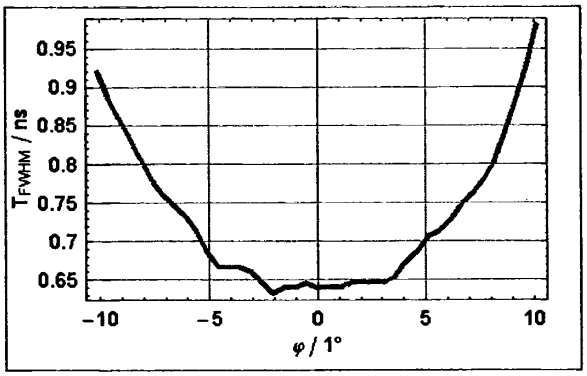

Figure 17: Pulse duration (T_{FWHM}) as a function of the direction angle in the horizontal plane

The measured values of the scan in the horizontal plane are shown in Figure 16 (peak electric field) and Figure 17 (pulse duration). Due to the symmetry of the antenna design the horizontal scan gives symmetric values with respect to $\varphi_h = 0°$. As expected the maximum peak electric value and the shortest pulse duration occur at $\varphi_h = 0°$.

The characteristic parameters of the short pulse simulator (measured and predicted) are given in Table 1. As discussed before deviations between the predicted and measured direction of the maximum peak electric field can be observed due to the short measurement distance. Nevertheless there is a good agreement between the measured transfer factor E_{max} / (U_0 m^{-1}) and the predicted far field values. If we take into account the near field behavior of aperture antennas [8] the measured values lead to a transfer factor of $E_0 / U_0 m^{-1} \approx 0.2 - 0.23$ at a distance of R = 40 m.

Table 1: Performance of the simulator

	Vertical		Horizontal
	measured (R = 11 m)	predicted (far field)	measured (R = 11 m)
direction of max. peak field	8°	1.5°	0°
spot size (50 % voltage)	±9°	5.0°	±10°
transfer factor (E_{max} / U_0 m^{-1})	0.22	0.22	0.22
direction of min. T_{FWHM}	4°	1.5°	0°
min. T_{FWHM}	0.65 ns	0.1 ns	0.65 ns

V CONCLUSION

In this paper the setup of a short pulse simulator system for susceptibility investigations is presented. The source produces pulses with an amplitude of 100 kV and a risetime of less than 500 ps. The generated pulses are radiated using a half reflector type IRA.

The comparison between computed field values and near field measurements shows a good agreement. Based on the presented behavior the short pulse simulator is able to generate transient electric fields with magnitudes of several kV/m at distances of up to 100 m. It can be used for further susceptibility investigation on modern electronics.

IV. REFERENCES

[1] W. Prather, F. Agee; Ultra Wideband Sources and Antennas, Ultra Wideband short pulse electromagnetics-4, 1998

[2] G. A. Mesyats, S. N. Rukin; Generation of high power subnanosecond pulses, Ultra Wideband short pulse electromagentics-4, 1998

[3] C. E. Baum, E. F. Farr Impulse radiating antennas, Ultra Wideband short pulse electromagentics-2, 1993

[4] E. G. Farr, C. A. Frost; Development of a Reflector IRA and a Solid Lens IRA, Part I: Design, Predictions and Construction, Sensor and Simulation Note 396, April 1996.

[5] E. G. Farr and C. E. Baum, Prepulse Associated with the TEM Feed of an Impulse Radiating Antenna, Sensor and Simulation Note 337, March 1992.

[6] M. Jung, Th. Weise, U. Braunsberger, F. Sabath; High Power Compact UWB-Systems, International Conference on Pulsed Power Applications, Gelsenkirchen, March 2001

[7] C. E. Baum, Radiation of impulse like transient fields, Sensor and Simulation Note 231, Nov. 1989

[8] D. V. Giri, J. M. Lehr, W. D. Prather, C. E. Baum, R. J. Torres, Intermediate and Far Fields of Reflector Antenna Energized by a Hydrogen Spark-Gap Switched Pulser, Transactions on Plasma Science; Vol. 28, No. 5. October 2000, pp. 1631-1636